Monthly Notices of the ROYAL ASTRONOMICAL SOCIETY

MNRAS **522,** 5758–5774 (2023) https://doi.org/10.1093/mnras/stad015
Advance Access publication 2023 January 11

Applying unsupervised learning to resolve evolutionary histories and explore the galaxy–halo connection in IllustrisTNG

T. S. Fraser,[1]★ R. Tojeiro [2] and H. G. Chittenden [2]

[1] *Waterloo Centre for Astrophysics, Department of Physics & Astronomy, University of Waterloo, 200 University Ave. W., Waterloo, Ontario N2L 3G1, Canada*
[2] *School of Physics & Astronomy, University of St Andrews, North Haugh, St Andrews KY16 9SS, UK*

Accepted 2022 December 19. Received 2022 December 17; in original form 2021 December 29

ABSTRACT

We examine the effectiveness of identifying distinct evolutionary histories in IllustrisTNG-100 galaxies using unsupervised machine learning with Gaussian mixture models. We focus on how clustering compressed metallicity histories and star formation histories produces sub-population of galaxies with distinct evolutionary properties (for both halo mass assembly and merger histories). By contrast, clustering with photometric colours fails to resolve such histories. We identify several populations of interest that reflect a variety of evolutionary scenarios supported by the literature. Notably, we identify a population of galaxies inhabiting the upper red sequence, $M_* > 10^{10}$ $M_{\odot,}$ that has a significantly higher *ex-situ* merger mass fraction present at fixed masses and a star formation history that has yet to fully quench, in contrast to an overlapping, satellite-dominated population along the red sequence, which is distinctly quiescent. Extending the clustering to study four clusters instead of three further divides quiescent galaxies, whereas star-forming ones are mostly contained in a single cluster, demonstrating a variety of supported pathways to quenching. In addition to these populations, we identify a handful of populations from our other clusters that are readily applicable to observational surveys, including a population related to post-starburst galaxies, allowing for possible extensions of this work in an observational context, and to corroborate results within the IllustrisTNG ecosystem.

Key words: methods: data analysis – galaxies: evolution – galaxies: formation.

1 INTRODUCTION

In concordance cosmology, galaxies form within dark matter haloes and follow hierarchical evolutionary histories (Cole et al. 2000). The so-called galaxy–halo connection is an umbrella term that attempts to capture the complex relationship between the evolution of galaxies and their haloes (e.g. Wechsler & Tinker 2018). For example, the observed spatial distribution of galaxies is reasonably well modelled by populating dark matter haloes of different masses (and other properties, such as age) with different types of galaxies (e.g. Zehavi et al. 2005; Guo et al. 2014), and the role of mergers – a prominent prediction of hierarchical structure formation – has long been considered in the growth of galaxies (e.g. Wake et al. 2006; Bundy et al. 2009; Tojeiro et al. 2012; Moustakas et al. 2013), galaxy morphological transformation (e.g. Bertone & Conselice 2009; Martin et al. 2018), the quenching of star formation (e.g. Pawlik et al. 2018), or the onset of active galactic nuclei (AGNs) (e.g. Villforth et al. 2014). However, the evolution of haloes is not directly observable, and the evolution of galaxies is only partially observable: star formation and metallicity histories give key insights into major evolutionary events, but do not account for the entirety of it. Cosmological hydrodynamic simulations have shown that star formation histories (SFHs) are extraordinarily sensitive to a variety of factors and consequently produce a large scatter driven by these parameters, rendering evolutionary descriptions incomplete (e.g. Lagos et al. 2016; Diemer et al. 2017; Cochrane & Best 2018).

Simulations allow for non-observable halo and galaxy properties to be considered in the context of their evolution; e.g. dark matter, local environment, halo concentration, and halo mass assembly histories (MAHs) have been successfully modelled. As a consequence, as simulated galaxies begin to match observed galaxies on a range of properties and redshifts (e.g. Henriques et al. 2015; Pillepich et al. 2017a; Davé et al. 2019), questions regarding the impact of halo evolution on the evolutionary histories of galaxies can be explored. Given the large parameter space that galaxy observables occupy, simulations can be used to explore emergent relationships between different parameters, which were not originally considered (e.g. Tojeiro et al. 2017).

Simulations like IllustrisTNG (Nelson et al. 2017, 2018; Pillepich et al. 2017b; Springel et al. 2017; Marinacci et al. 2018; Naiman et al. 2018), EAGLE (Schaye et al. 2014), and SIMBA (Davé et al. 2019), and their associated bodies of literature present a remarkable opportunity, as they contain thousands of simulated galaxies, with a multitude of observable and non-observable parameters, governed by a vast array of non-linear, multivariate relationships. This has led to work that explored the use of unsupervised learning techniques to uncover data-driven relationships that we would not be privy to a priori. One source of success was in applying dimensionality reduction, through the form of principal component analysis (PCA), which has seen application to a wide variety of fields in astrophysics and in galaxy evolution. Dimensionality reduction can result in the discovery of physically driven mechanisms present in galaxies and allows us to quantify them. Lagos et al. (2016), through use of PCA, uncovered a 'fundamental plane' of star-forming galaxies,

★ E-mail: tsfraser@uwaterloo.ca

driven by a correlation between the star formation rate, the neutral gas fraction, and the stellar mass. These three variables were seen to account for the majority of the variance seen in galaxies, and the authors were able to interpret the shape of this fundamental plane as a result of the self-regulation of the galaxies' star formation rates. Another example of the use of PCA in studying relationships between galaxy observables is Cochrane & Best (2018), which again employed EAGLE simulation data to study connections between the star formation rate, dark matter halo mass, and stellar mass across redshifts. These connections were further examined by splitting of galaxies as centrals or satellites, and according to their stellar mass. This sort of analysis is pertinent for us given that it directly links the SFH with halo parameters, and the PCA seems to suggest a few physically driven mechanisms at work. The relative strength of this M_*-M_h-SFR relation varies based on the galaxy's mass and central/satellite status, which implies that the driving variables of the SFH, and their link to the halo, might vary based on the type of galaxy, in addition to highlighting differences in quenching regimes.

The scatter in SFHs, for galaxies of similar mass, has also been studied using simulations. Sparre et al. (2015), using PCA on the Illustris simulation, argue that variability on scales above or below 500 Myr is likely related to different processes, with halo assembly histories responsible for long time-scale variations and gas accretion for short time-scale effects. Diemer et al. (2017) fitting SFHs using log-normals found that the scatter in SFHs could not be uniquely determined by a single parameter. Cohn (2018), building off of this work, compared Diemer et al.'s (2017) lognormal model to that developed with PCA. Although PCA is able to reproduce simulated SFHs, the authors point out that the underlying assumption of PCA – that scatter seen in the simulation is but a deviation from a single underlying SFH – is unlikely to be true. Rather, Cohn states: 'It is possible to group galaxies into more than two sub-families, with each sub-family having similar integrated SFR histories'. Additional support for this diversity of groups of formation histories is seen in Carnall et al. (2018). Taken together, these studies propose that we do not interpret formation histories and their scatter as deviations from a single, underlying, general SFH, but instead consider the existence of a series of sub-families, each with different SFHs, and scatter. This is where the case for unsupervised learning via clustering is strong: as small populations can contribute little to the overall variance, but can be distinct and of astrophysical interest.

This sensitivity problem is not unique to SFHs. Halo assembly histories have consistently demonstrated a multivariate sensitivity to other parameters. Wang et al. (2020) underscore the importance of parametrizing the MAH, as even the occurrence of minor merger events along the evolutionary history of the halo can drastically alter its structure. They note even small amounts of accretion can alter the concentration, therein driving the scatter in the MAH, further affecting other halo parameters. Obreschkow et al. (2020) and Chen et al. (2020) both emphasize the importance of using the full merger tree for understanding halo evolution, outlining a major challenge in linking the MAHs to SFHs, as even subtle differences in parametrization can have drastic effects.

The sensitivity of MAHs also affects the baryonic components of galaxies. Rey, Pontzen & Saintonge (2019) find that MAHs are enormously sensitive to initial conditions, and that this sensitivity is extremely influential on the SFH. In particular, they propose that the larger scatter in SFHs may be partially driven by the sensitivity of MAHs to parameters surrounding mergers.

Chen et al. (2020) address the sheer diversity of non-observable parameters that can be used to describe dark matter haloes and their MAHs. They outline a variety of possible parametrizations of the MAH of haloes and uncover a tight correlation between the MAH of the halo and its concentration. Their analysis finds that more than 80 per cent of the variance is explained by the MAH. As stated previously, this means that the scatter of SFHs is not wholly determined by baryonic processes, as the halo assembly history also influences the scatter seen in the SFHs, illustrating the influence the galaxy–halo connection has on these sensitive parameters.

In this paper, we will use the IllustrisTNG-100 simulation to explore a wide array of observable properties, including but not limited to SFHs, and use non-supervised machine learning (clustering) to identify sub-families (clusters) of galaxies. Critically, we will develop an analysis that allows us to take advantage of the observability of star formation and metallicity histories (see Hahn et al. 2022) and, through clustering, allows us to directly identify sub-populations of interest in future surveys. This work does not rank observables used in clustering per se, but instead focuses on the populations of interest that may be extracted. Given existing literature on the driving variables of dark matter haloes, we then aim to link these identified sub-families to different features of the MAH of the dark matter haloes and other halo parameters. Our research questions are as follows: (1) Can non-supervised clustering using galaxy observables reveal distinct populations in terms of their dark matter evolution? (2) How do those populations change according to the observables being clustered?

We consider two classes of observables: optical broad-band colours and compressed star formation and chemical enrichment histories. Time-resolved star formation and metallicity histories are often obtained from optical spectra, sometimes in conjunction with broad-band photometry (e.g. Tojeiro et al. 2017; Carnall et al. 2018; Hahn et al. 2022). Evidence shows that the addition of spectra has an important impact on the fitting process, either by mitigating the effects of the chosen priors or parametrization (Hahn et al. 2022) or by significantly sharpening the posteriors (Wild et al. 2020). We might therefore expect that clustering using star formation and metallicity histories allows a more detailed separation of galaxy populations.

This paper is organized as follows: Section 2 will detail the conceptual framework of unsupervised learning and the specific techniques used in this work. Section 3 will describe the data pipeline used to extract IllustrisTNG-100 data and the subsequent steps needed for use in our clustering, and describe the motivation for these steps, as well as the framework used to select the number of clusters. Section 4 will describe the results of our clustering and highlight the demographics of the sub-populations identified, and how these populations relate to the evolutionary history of these galaxies' dark matter haloes and merger histories. Section 5 will describe the characteristics of the sub-populations previously identified and place these results in context of the literature and discuss the role of different data sets. Section 6 will present the main conclusions of this work and outline areas that are promising for future work, both in the context of existing simulations and with observational data.

2 MACHINE LEARNING FRAMEWORK

Unsupervised learning was favoured here over more traditional forms of machine learning (e.g. supervised) owing to the transferability of results from observables to non-observables. By clustering, cluster membership can then be cross-referenced with dark matter halo properties of the IllustrisTNG simulation, without ever using them as a clustering variable, allowing us to probe the link between observables and dark matter halo features.

Clustering algorithms are effective at identifying distinct populations within a data set, defined here as populations that separate in a given parameter space. They are chosen over e.g. PCA for their ability to identify small distinct populations that may not contribute meaningfully to data set variance, but might otherwise be of interest to us.

2.1 Dimensionality reduction

The primary objective of dimensionality reduction is to represent a large, multivariate data set in a lower dimensional space. This is primarily achieved by constructing a basis that will adequately represent a D-dimensional data set in d dimensions. Two common methods of achieving this are via PCA and non-negative matrix factorization (NMF), both of which are methods that decompose the data into a series of basis vectors.

The use of dimensionality reduction with our IllustrisTNG data was strongly motivated by our interest in the star formation and metallicity histories and their roles in determining different subpopulations. The distribution of stellar ages and their metallicity can be recovered from the simulation with almost arbitrarily high resolution, making the problem intractable from a clustering perspective. At the same time, Hahn et al. (2022) demonstrate the validity of using compressed star formation and metallicity histories as the basis vectors for a non-parametric model of the spectral energy distribution (SED) of galaxies. NMF coefficients are being directly fitted to 10 million low-redshift galaxies observed by the Dark Energy Spectroscopic Instrument (Hahn et al. 2022), creating a population of real galaxies with which our results can be compared. We use NMF components to represent the star formation and metallicity histories and smoothed on scales of 414 Myr (three bins), to construct our basis.

In addition, we use PCA to gauge the distinctness of the clusters we produce, by comparing the basis vectors. We refer the reader to Shlens's (2014) tutorial and Ivezić et al.'s (2014) section on PCA for a detailed overview. For NMF, we refer the reader to Ivezić et al. (2014) and Zhu (2016), as this method has often seen use in representing galaxy SEDs, among other applications, and provides a technical overview. For both of these methods, we made use of the built-in implementations offerred by sklearn (Pedregosa et al. 2011).

2.2 Expectation maximization

As described in Section 3, we ultimately settled on a Gaussian mixture model (GMM) as our clustering algorithm of choice. We made use of the implementation of GMM offered by sklearn (Pedregosa et al. 2011). Expectation maximization (EM) is the core method that governs clustering in several algorithms, including GMM. Here, we overview its underlying concept.

EM works by making an initial estimate of the posterior probability [the probability of a data vector x_i being in cluster j: $p(j|x_i)$], which can then be used to find the corresponding parameters of the distribution. Using these parameters, the probability is updated (the expectation step). These steps are repeated until it converges on a local maximum, which effectively means that each data vector, x_i, now has an associated cluster membership, j. In the case of GMM, $p(j|x_i)$ is a Gaussian, but this takes on a more general form for other algorithms using EM, with starting point being the partial derivatives of the log likelihood of a given probability distribution (being Gaussian in this case).

See Cohn (2018) for a caution against modelling individual SFHs as perturbations around a single mean.

Table 1. Table of supplementary catalogues used for variables either in the clustering, or in post-clustering analysis. Catalogues cited as advised by IllustrisTNG. Catalogue G is from Rodriguez-Gomez et al. (2015, 2016, 2017), and catalogue K is from Nelson et al. (2017) and sources therein. The photometry and colours from catalogue K use ugriz Sloan Digital Sky Survey (SDSS) rest-frame bands and a separate entry of *UJV* bands (rest frame, but not used for this analysis). The dust model accounts for effects of obscuration, and is specifically model 'C' from Nelson et al. (2017), which is their resolved dust model. For $z = 0$, this photometry is provided as a series of absolute magnitudes.

Catalogue index	Catalogue name	Variables used
G	Stellar assembly	$f_{\rm InSit}, f_{\rm Outgal}, f_{\rm M}, f_{\rm Stripped}$
K	SDSS photometry, colours, and mock fibre spectra	SDSS *ugri* magnitudes

3 METHODS

IllustrisTNG is a suite of 29 cosmological hydrodynamic simulations of assorted volume, mass, and resolution. All IllustrisTNG simulations assume the Planck 2015 ΛCDM cosmological model (i.e. $\Omega_{\rm m} = 0.3089$, $\Omega_\Lambda = 0.6911$, $\Omega_{\rm b} = 0.0486$, $H_0 = 67.74$ km s^{-1} Mpc^{-1}) (Pillepich et al. 2017a).

The public data sets are divided into 100 'snapshots' in time, covering a redshift range of 0–20, with a mean separation in time of 137.6 Myr. Each halo has an associated merger tree, detailing the properties of the numerous progenitors of the halo at prior snapshots of the simulation (Jiang & van den Bosch 2014; Nelson et al. 2019). This work considers the mass assembly and merger history of central haloes along the main progenitor branch (MPB) of the tree, i.e. the history specific to the most massive halo at each snapshot.

IllustrisTNG is run on three volumes. The runs are denoted as TNG-50, TNG-100, and TNG-300, which are approximately 50, 100, and 300 Mpc across, respectively. TNG-300 has the largest sample of galaxies, at the cost of the lowest resolution, suited for high-mass objects. By contrast, TNG-50 is more suited for studying internal processes of galaxies and the structures of individual subhaloes (Nelson et al. 2018). We opted to use the TNG-100 simulation, balancing statistics with resolution. IllustrisTNG incorporates supermassive black hole feedback, primordial magnetic fields, and an upgraded galaxy evolution model (see Nelson et al. 2018 for details).

3.1 Data extraction: baryonic properties

We took a mass cut of galaxies of $\log M_*/{\rm M}_\odot > 9.5$ at the final snapshot ($z = 0$), giving a total of 12 535 galaxies.

We extracted the ages and metallicity of all stellar particles bound to each sub-halo in our sample, up to two effective radii. The SFHs were computed as the mass formed in each of 100 bins of lookback time, linearly spaced between 0 and the age of the Universe at $z = 0$. The metallicity histories were computed by taking the the mass-weighted metallicity in the same bins. Metallicity is defined as the mass fraction in elements heavier than He. We complemented our data with TNG public catalogues; these are summarized in Table 1.

3.2 Pre-processing

We compressed the SFHs using NMF, in order to reduce the dimensionality of our data. We prefer to use NMF over, for example, PCA, due to the non-negativity constraints on the basis vectors. Doing so allows us to interpret basis vectors physically, as stellar mass or metallicity.

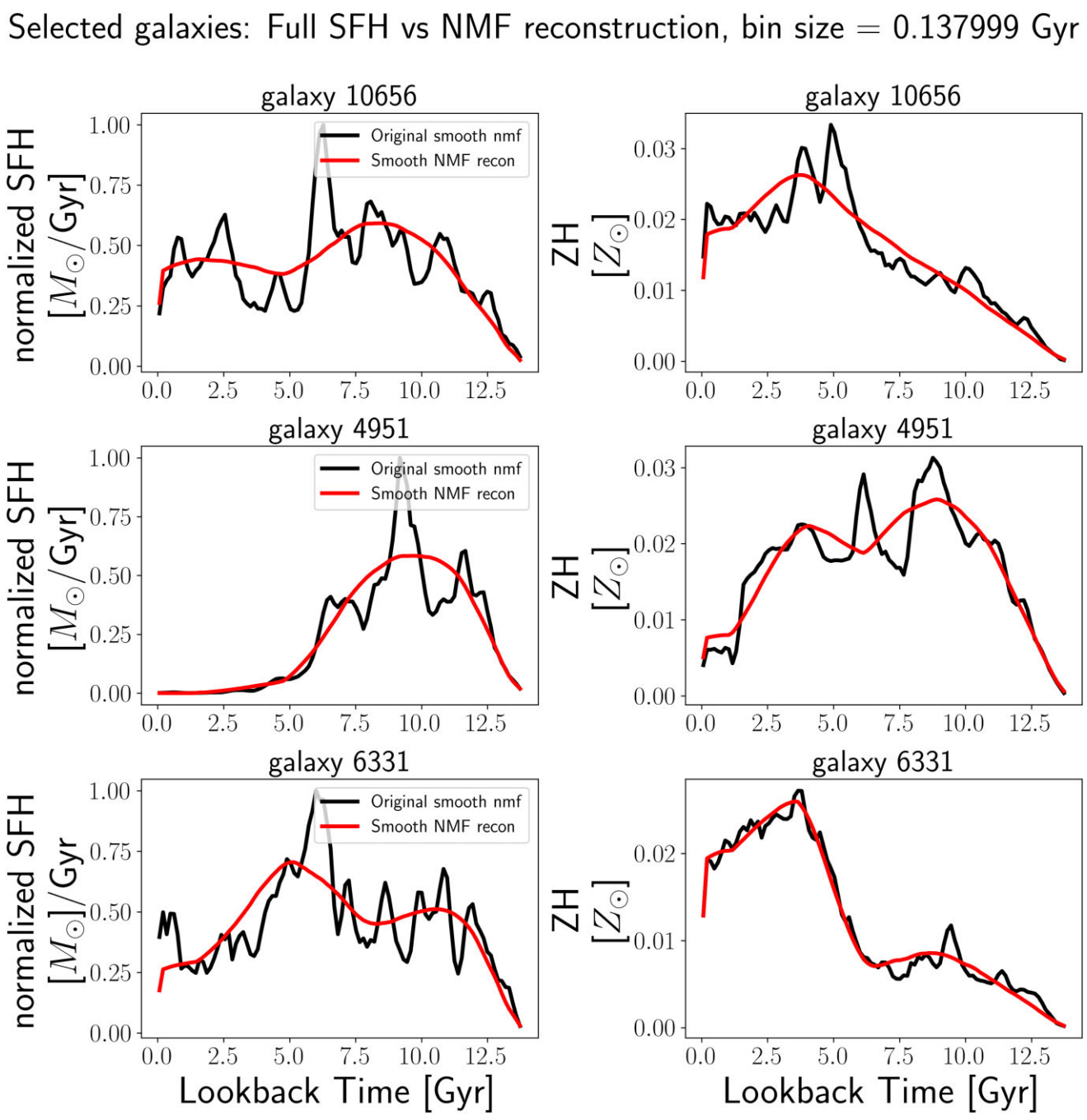

Figure 1. Plot of three reconstructed SFHs and metallicity histories, smoothed and decomposed into four NMF components. Generally, the overall behaviour of the SFHs is captured, and the integrated stellar mass of the reconstruction is consistent with the original integrated stellar mass of Fig. 2.

To ensure that the NMF preserves the major features and relationships in the SFHs, we normalize the star formation using a maximum absolute value normalization. This ensures that the maximal value of an individual galaxy's SFH is 1 and minimum is at 0.

We determined the number of components needed by comparing NMF-reconstructed SFHs with the originals. At around four components, we are able to sufficiently reconstruct most SFHs (see Fig. 1). Their integral gives a stellar mass within 0.1 dex of the original, in line with observational uncertainties (see Fig. 2). Specifically, we find only 2 galaxies with integrated stellar masses away from the original by 0.2 dex, and 47 away from the original by 0.1 dex. None exceeds a deviation of 0.21 dex. This methodology was extended to metallicity histories, where we again found four components as being sufficient in representing the majority of metallicity histories. While we expect that a higher number of components would be needed to fit individual galaxies [e.g. Hahn et al. (2022) require a stochastic burst in addition to four smooth NMF components in order to reproduce realistic galaxies], populations of galaxies can be described by a smaller number of smooth components (Chaves-Montero & Hearin 2021).

Additional parametrizations for star formation and metallicity histories were explored, e.g. taking mass-weighted means of the metallicity, identifying the peak of the formation histories, comparing

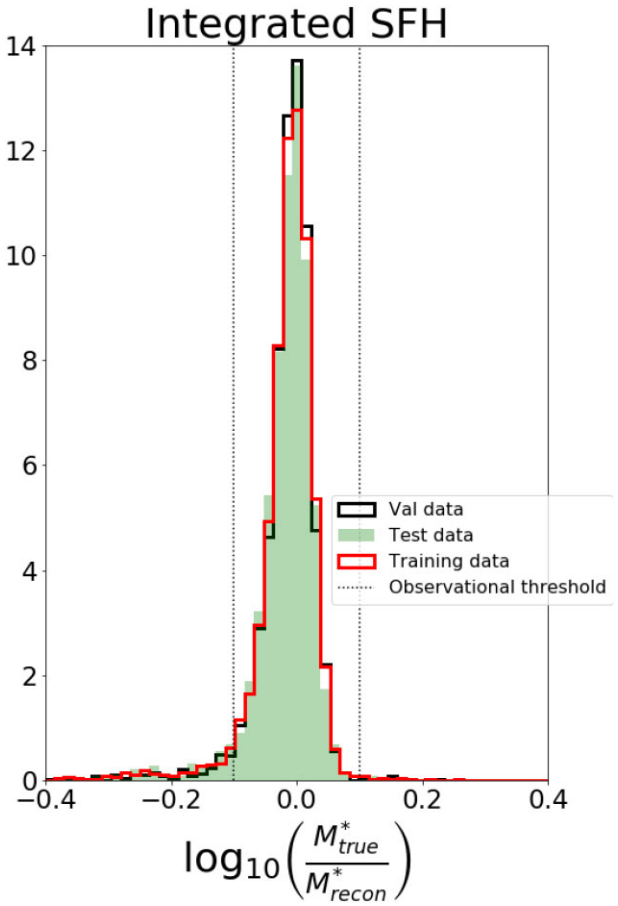

Figure 2. A normalized histogram of the integrated SFHs, comparing between the original SFHs and the reconstructed ones. Most (99 per cent) fall within the threshold of ±0.1 dex, with only a handful exceeding that, the greatest by no more than ±0.21 dex. The galaxy number does not correspond to the subhalo ID.

the timing of these peaks, and the net change in SFH between adjacent bins. Ultimately, while incorporating these parameters did contribute to an interesting set of clusters, we found these clusters could be partially reproduced through using a smaller parameter space, populated by NMF representations of the star formation and metallicity histories.

3.3 Data extraction: dark matter properties

We use the halo MAHs as computed in Chittenden & Tojeiro (2022) and summarize how they are computed in this section.

The dark matter halo's mass accretion rate is defined using the Friends-of-Friends (FoF) group mass enclosed within a sphere whose density is 200 times the cosmic critical density at the given time, and whose radius is defined accordingly. We convert this to the rate of accretion onto the halo by finite differencing along the MPB with respect to the time t_i at each snapshot, per equation (1).

$$\dot{M}_h(t_i) = \frac{M_h(t_i) - M_h(t_{i-1})}{t_i - t_{i-1}}. \quad (1)$$

The amplitude and geometry of such accretion rates are useful indicators of the manner of ongoing halo formation. Smooth accretion of dark matter is usually characterized by small gradients in the accretion rate, whereas merger events present more instantaneous or sharply rising peaks.

3.4 Defining clusters

We considered and tested a number of clustering algorithms. We did this by clustering a subset of our parameter space: the peak star formation rate, mass-weighted mean metallicity, and stellar mass – a compressed representation of the parameter space we wanted to explore. We found that GMMs were preferable, as the cluster labels they produced cluster with distinct populations that aligned with the results of visual inspection, which is feasible in a low-dimensional parameter space. Next, we had to decide on the number of clusters, as EM algorithms like GMM require this to be dictated a priori. Scoring metrics assign a score to a set of clusters, according to Pedregosa et al.'s (2011) implementation of the Silhouette score (Rousseeuw 1987), Calinski–Harabasz index (Caliński & Harabasz 1974), and the Davies–Bouldin Index (Davies & Bouldin 1979). Although scoring metrics attempt to determine the optimal number of clusters, their accuracy is questionable – in our tests, different metrics often produce different results. Instead, we developed a 'consensus framework' consisting of the following steps:

(i) Clustering the entire data set with $N = 2\,M_{\rm BIC}$ clusters, where $M_{\rm BIC}$ is the number of clusters as recommended by the Bayesian information criterion (BIC). BIC assumes a Gaussian distribution, and penalizes overfitting; therefore, the number of components that extremizes the BIC is the upper limit, as it assumes fully Gaussian data (Ivezić et al. 2014).

(ii) Scores are computed for different metrics (Silhouette score, Calinski–Harabasz index, and the Davies–Bouldin index). Each recommends a certain number of clusters.

(iii) If the number of clusters suggested by all three metrics is the same, then there is a clear agreement on the clustering, and we run through it with the validation set to verify and use it as the definitive set of clusters.

(iv) If the number of clusters is in agreement, but not in consensus (i.e. a 2–1 vote), we use the validity index, a scoring system defined by Moulavi et al. (2014). If there is still no agreement, then it merits further visual inspection. A final decision is made based on visual inspection.

We consistently found three and four clusters as being a well-supported choice. It also produced clusters whose parameter distribution appeared reasonable under visual inspection. The selection of three or four clusters is not wholly authoritative, as other clusterings could still be found to have distinct populations – the number of suggested clusters ranged from 2 to 5, depending on the score.

We argue that our methodology supports the choice of three and four clusters, which we also confirmed by investigating if they are distinct via PCA.

We ran PCA on each cluster and on the entire population of galaxies. Comparing the eigenvectors in each case allows us to determine whether the sub-population being surveyed is distinct from the overall population.

Fig. 3 demonstrates this process. We first sub-divide our data set into four populations, each with a corresponding number of galaxies as in our clusters, but the galaxies themselves randomly selected. We then run a Monte Carlo simulation of the PCA on these facsimile sub-population, recording their eigenvectors. We then take our clusters and run PCA on each of them, in the same manner (50 000 times for each sub-population). We ran it 50 000 times for the randomly sampled subsets (black), and the clustered populations (colour) in the resulting eigenvectors are plotted in Fig. 3. Seeing how the distributions of both the random sub-sample's PCA and the corresponding sub-population's PCA vary, we can then conclude

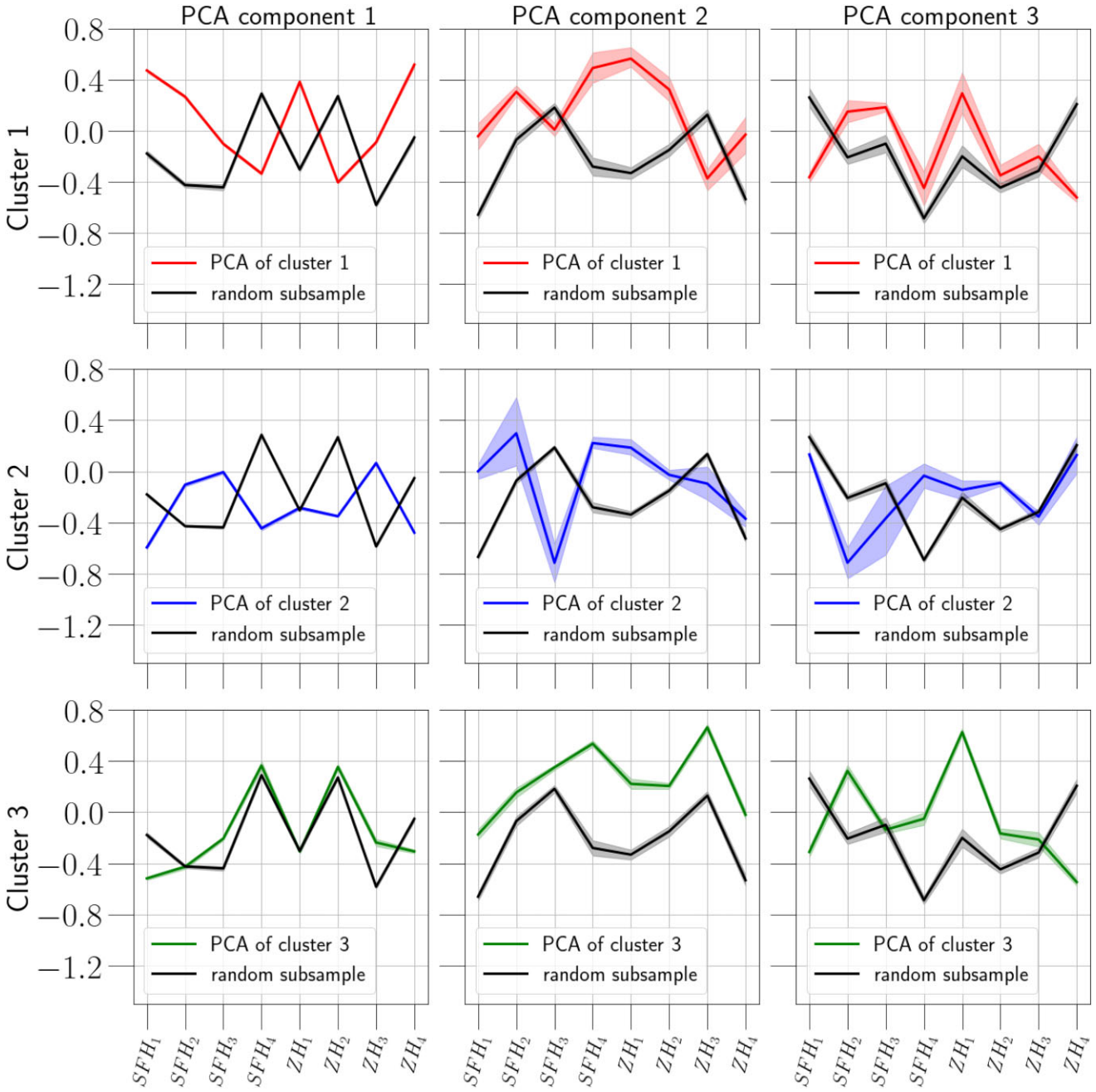

Figure 3. Comparison of the PCA eigenvectors of both a given cluster (run 50 000 times) and a randomized subset of galaxies from IllustrisTNG. The shaded regions are the 5th/95th percentiles and demonstrate that each cluster consists of populations whose PCA components do not fully overlap with each other, nor do they resemble the general population of 12 535 galaxies used. This is how we establish that the sub-populations (as identified by our clusters) are distinct. The dark lines and their shaded regions are random equivalents of a selected population (i.e. a random subsample of galaxies, selected without the cluster labels, was selected and run through the same procedure, to demonstrate that the populations identified differ from a random subsample).

that these populations are considered 'distinct'. Although only shown here for one case, we perform an equivalent PCA on all cluster sets detailed in the next section.

3.5 Procedure

Our analysis worked in two stages. First, we determined clusters with 'observables' from IllustrisTNG. We defined sets of clusters based on the NMF compression of star formation and metallicity histories and/or optical colour – see Table 2 for a summary. Secondly, we linked these clusters to dark matter halo parameters: the mass-weighted age, the halo MAH, the stellar *in/ex-situ* mass fractions, and the dark matter fraction.

We also select for central and satellite galaxies by defining centrals as the most massive subhalo in a given group in the *FoF haloes* group catalogue. All other galaxies are treated as satellites. The breakdown of centrals and satellites is outlined in Table 3. We can then cluster the data and determine the cluster labels for the full data set and apply the central/satellite splits. We evaluated the similarity of these distributions by also comparing the results of a two-sided

Table 2. Key features of each cluster set: their dimensionality (number of parameters clustered), the number of clusters produced, and a short description of the parameter space.

Case	Number of clusters	Dimensions	Description
A	3	3	Populations from clustering three photometric colours $u-g$, $g-r$, and $r-i$.
B	3	8	Populations from clustering NMF compressions of star formation and metallicity histories.
C	3	11	Populations from clustering with parameter space of cases A and B.
D	4	3	Populations from clustering three photometric colours $u-g$, $g-r$, and $r-i$.
E	4	8	Populations from clustering NMF compressions of star formation and metallicity histories.
F	4	11	Populations from clustering with parameter space of cases D and E.

Table 3. Summary table of each of the six cases explored in this work. Here, we enumerate the number of galaxies that were identified in a given case as central or satellite, and their breakdown across clusters. While there are some differences between our major cases of interest (cases B, C, E, and F), we can see some analogous features. In particular, the satellite dominance of one of the clustered populations, typically inhabiting the lower red sequence, is readily apparent for cases B and C.

Case	Cluster	$N_{\rm Centrals}$	$N_{\rm Satellites}$	%Centrals	%Satellites
A	1	1043	2048	33.74	66.26
A	2	4523	1628	73.53	26.47
A	3	1671	1622	50.74	49.26
B	1	390	1464	21.04	78.96
B	2	5200	2696	65.86	34.14
B	3	1647	1138	59.14	40.86
C	1	5193	2333	69.00	31.00
C	2	760	1723	30.61	69.39
C	3	1284	1242	50.83	49.17
D	1	179	372	32.49	67.51
D	2	930	1830	33.70	66.30
D	3	5121	1879	73.16	26.84
D	4	1007	1217	45.28	54.72
E	1	3369	1737	65.98	34.02
E	2	96	701	12.05	87.95
E	3	2804	1664	62.76	37.24
E	4	968	1196	44.73	55.27
F	1	5022	2259	68.97	31.03
F	2	714	1091	39.56	60.44
F	3	1405	1245	53.02	46.98
F	4	96	703	12.02	87.98

Kolmogorov–Smirnov (KS) test on the *ex-situ* mass fractions from mergers. This is because almost all the galaxies in our population have a non-zero *ex-situ* mass fraction from mergers, so comparing the KS test result for these statistics is critical. Our criterion for similarity was defined as the two-sided KS test producing a p-value of greater than 0.05.

4 RESULTS

Fig. 4 visualizes all of our cluster sets (as described in Table 2) as colour–stellar mass plots. Stellar mass was not used in the clustering, and optical $g-r$ colour was only used in some of the sets. We show a colour–stellar mass diagram to situate the discussion, which we will often phrase in terms of a red sequence, a blue cloud, or a green valley. We outline the general description of each case and cluster in Tables 3 and 4, and a breakdown of their central/satellite membership.

For a more exhaustive overview of each section, we refer the reader to the subsections below. We ordered these subsections based on their importance to our task of identifying distinct populations.

Throughout our discussion of each set of clusters, we will refer to plots of mean SFHs, metallicity histories, halo assembly histories, and histograms of the fraction of stellar mass assembled *ex-situ* by mergers and flybys. We diminish the role of stellar mass in our results by focusing our discussion – and our plots – in a fixed stellar mass interval, corresponding to 10–11 in $\log M_*/\mathrm{M}_\odot$. This interval samples most of our clusters well while avoiding the extremes of the galaxy population. We have kept a consistent colour scheme in all plots, such that red represents the most quenched population, blue the most star-forming population, and green the remaining population. In the case of four clusters, we have represented the new population in pink.

We found that clusters determined using the star formation and metallicity histories were especially effective in identifying populations with distinct evolutionary histories. By contrast, clustering with broad-band colours while effective in differentiating between different SFHs was not as effective in distinguishing other evolutionary aspects. Here, we will highlight the different clusters we found and summarize their features, both observable and non-observable, and how that distinguishes their respective evolutionary histories. We find that cases A and D with photometric colours produce only superficial distinctions in their populations as we discuss below. We also find that case C fails the two-sided KS test, as the probability of two distributions being drawn from the same probability distribution function is significant ($p > 0.05$). For case F, this complicates comparisons with case C, so we opt to study cases B and E in greater detail, and place them first in this section.

4.1 NMF-derived clusters – case B

The mean star formation and metallicity histories of each cluster are shown in Fig. 5, the dark matter halo assembly histories in Fig. 6, and the fraction of mass accreted by mergers and flybys in Fig. 8.

In the colour–mass diagram (Fig. 4), we found that the clusters split along the lines of a star-forming, blue cloud population of galaxies (cluster 2), with two other clusters coming from a split in the 'red sequence' population of quiescent galaxies, largely corresponding to their stellar mass, but not entirely driven by it. In the mass range of 10–11 dex, one such sub-population (cluster 1) is satellite dominated (78.96 per cent) with a late peak in its MAH at approximately 6 Gyr in lookback time, while the other is primarily dominated by central galaxies with a consistently higher *ex-situ* mass fraction, sourced from mergers (cluster 3); see Fig. 8 for reference. Moreover, the mass-weighted ages of the stellar matter and the dark matter haloes can be taken in contrast with each other to highlight differences in the formation histories of these populations. In cluster 1, the halo mass-weighted age is $7.68^{+1.45}_{-1.33}$ Gyr, whereas its stellar mass-weighted age is $9.91^{+1.26}_{-1.29}$ Gyr, indicating that most of the star formation seems to precede significant growth of the final halo. As convention, we

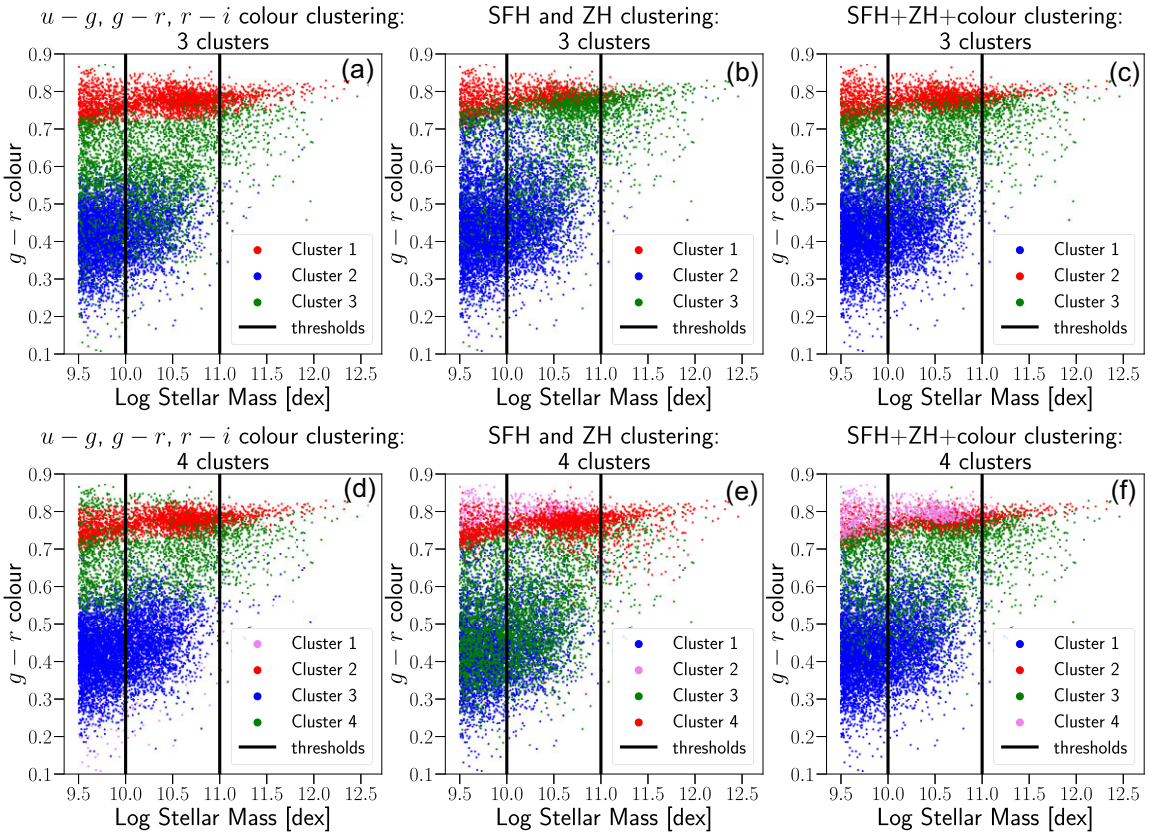

Figure 4. Colour–mass plot of the six different cases we explored in detail. This plot serves to situate the reader, covering the different clusterings we explored. These cases were the clusters that emerge when clustering $u-g$, $g-r$, and $r-i$ colours (left column), as well as NMF-4 component representations of the star formation and metallicity history (middle column), and the result of clustering the latter together (right column). The top row focuses on cases with three clusters, and the bottom row focuses on cases with four clusters. Generally speaking, while there are a great deal of similarities between cases, this colour–mass plot only serves to situate the reader, as other metrics were needed to quantify the differences in these evolutionary histories. The black lines denote the mass range used for our fixed-mass figures.

Table 4. Summary table of the populations identified in Fig. 4, and the general descriptions of each of the clusters produced by our GMM. See Section 4 for a qualitative breakdown.

Case	Cluster 1	Cluster 2	Cluster 3	Cluster 4
A	Red sequence population of galaxies: quiescent and high $g-r$ colour.	Blue cloud population of galaxies: star-forming and younger.	Green valley population of galaxies.	
B	Low-mass red sequence population of galaxies mostly satellite dominated, with some overlap with cluster 3 in terms of mass, but with some drastic differences in its evolutionary history.	Blue cloud, primarily populated with star-forming galaxies and some galaxies inhabiting the 'green valley'.	High-mass red sequence population, tapers off below stellar masses of 10.5 dex, with considerable overlap with cluster 1 of this population. Primarily dominated by centrals.	
C	Blue cloud population of star-forming galaxies.	Red sequence population of galaxies, mostly quiescent.	Green valley population of star-forming galaxies.	
D	Sub-population of blue cloud population of galaxies, across various masses and parts of the colour gradient.	Red sequence population of galaxies: quiescent and high $g-r$ colour.	Blue cloud population of galaxies: star-forming and younger.	Green valley population of galaxies in addition to some redder galaxies.
E	Blue cloud population of galaxies. Relatively active star-forming population.	Very red subset of the red sequence. Predominantly lower mass galaxies up until 11 dex.	Green valley population, with some galaxies from upper red sequence.	Mostly red sequence galaxies ranging from low to high mass.
F	Blue cloud population of galaxies, generally a star-forming population.	Portion of the red sequence across all masses, excludes less red portion. Relatively narrow range of $g-r$ colour.	A segment of the red sequence, across all masses, notably excludes some redder, less massive galaxies.	Segment of lower red sequence, typically a much redder population (in terms of $g-r$ colour).

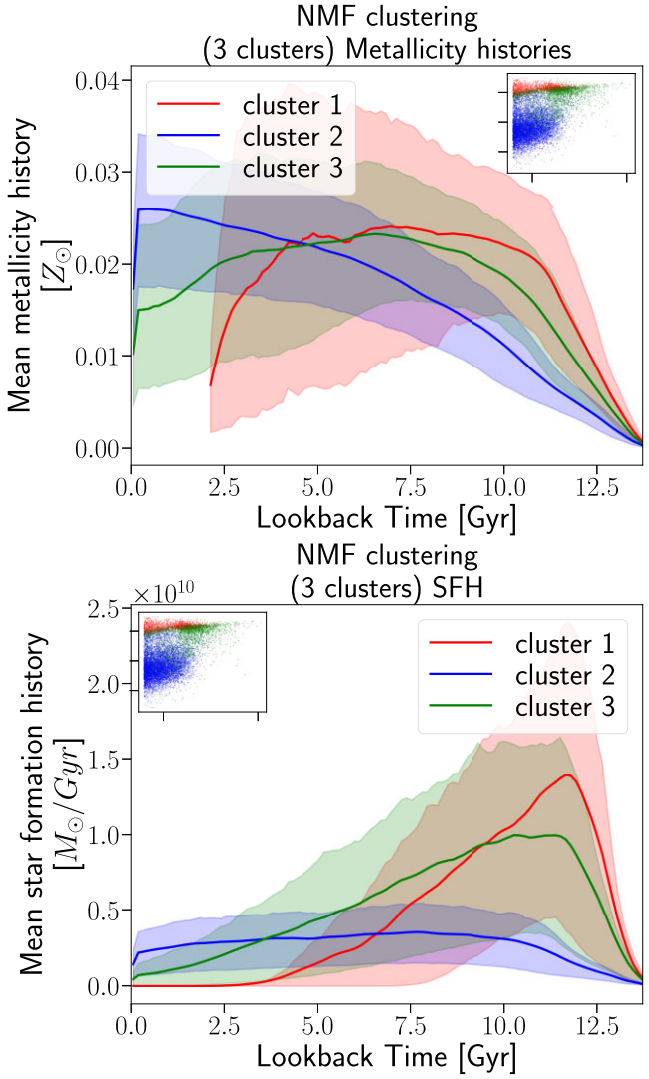

Figure 5. Case B: Clusters generated using smoothed NMF components of the star formation and metallicity histories. The ensuing populations are distinct in terms of both metallicity histories and SFHs, with the most striking feature being a division of the red sequence, with the upper portion (higher mass) having yet to fully quench, even along a fixed mass interval. Galaxies in this upper population (cluster 3) clearly seem to be experiencing something that prevents them from quenching as quickly as those seen in cluster 1. See Section 5 for more details.

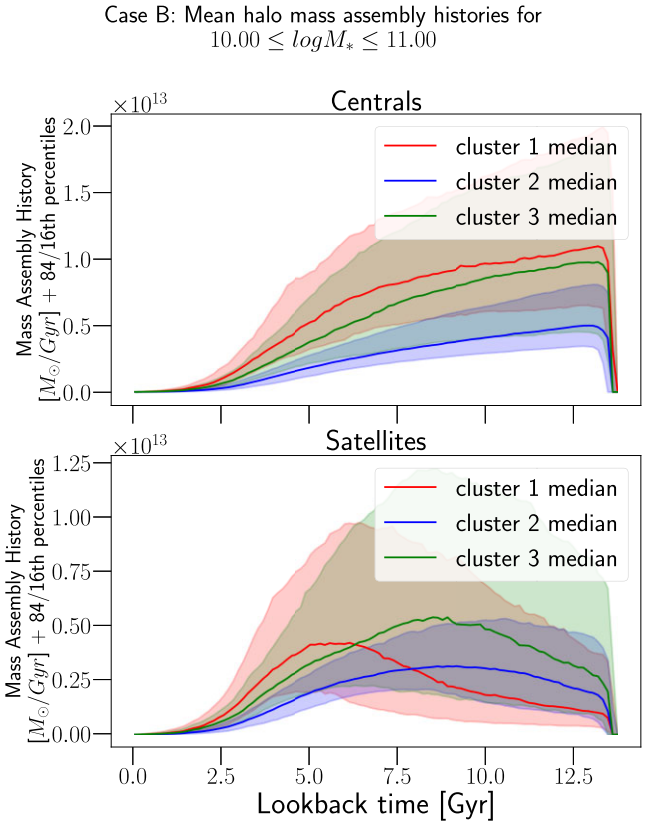

Figure 6. Case B: Median MAHs of the dark matter haloes of the galaxies from case B, with 1σ values shaded in. Here, we find that like all other cases, the greatest differences can be seen in the halo MAH of the satellite galaxies of a given cluster, rather than their centrals. We find that besides a slight variation in the overlap of median histories of clusters 1 and 3 for their centrals, the histories of the central galaxies barely vary, peaking early and diminishing as we approach the present. By contrast, the satellites in each of these clusters have distinct periods of time at which their MAHs peak (lower panel). The satellite-dominated population of cluster 1 peaks the most recently, approximately 6 Gyr ago. Meanwhile, merger-rich cluster 3 peaks further in the past, at 8 Gyr lookback time. These peaks might be suggestive of a period of more active mergers occurring for these respective galaxies, per Fig. 5 at these times. It is also demonstrative of the underlying differences identified by our clustering. Note that the solid line is a median.

denote the mass-weighted quantities with their mean age and their 16th/84th percentiles.

4.2 NMF-derived clusters – case E

By re-running the clustering for four clusters, we can explore what additional sub-populations might be lurking in our data set, and what features might distinguish them. The mean star formation and metallicity histories of each cluster are shown in Fig. 9, the dark matter halo assembly histories in Fig. 7, and the fraction of mass accreted by mergers and flybys in Fig. 11. It is important to note that adding a cluster means that the data set as a whole is re-clustered, meaning that some of the populations identified in a three-cluster case may not persist in a four-cluster case.

Adding a fourth cluster produces a population that begins to significantly quench 8–6 Gyr ago, using Fig. 9 as a reference. This also means we get a population quenching 5–2 Gyr ago, and another just beginning to quench around 0.5–1 Gyr ago. The final population best fits the characteristics of a blue cloud population: star formation is continuing relatively unabated.

This sub-population that quenched long before the others is extremely satellite dominated (87.95 per cent) compared to the other populations, but also a relatively small sub-population (797 galaxies out of a set of 12 535; see Table 4). It has the greatest difference in median *ex-situ* mass fraction for mergers (half an order of magnitude), and second largest for flybys, indicating that this is a population where mergers play a critical role in its evolution, and is more akin to other populations that are merger driven, i.e. cluster 4. What is notable as well, considering clusters 1, 2, and 3, is that while the mean SFHs all peak at similar times, their quenching time-scale as a population varies greatly. Moreover, we find in terms of mass-weighted ages for the halo and stellar mass, only clusters 1 and 3 have an older mass-weighted stellar age than halo age, with a difference of over 3 Gyr for cluster 1. This seems to indicate that most of the stars have formed prior to the final halo being fully assembled.

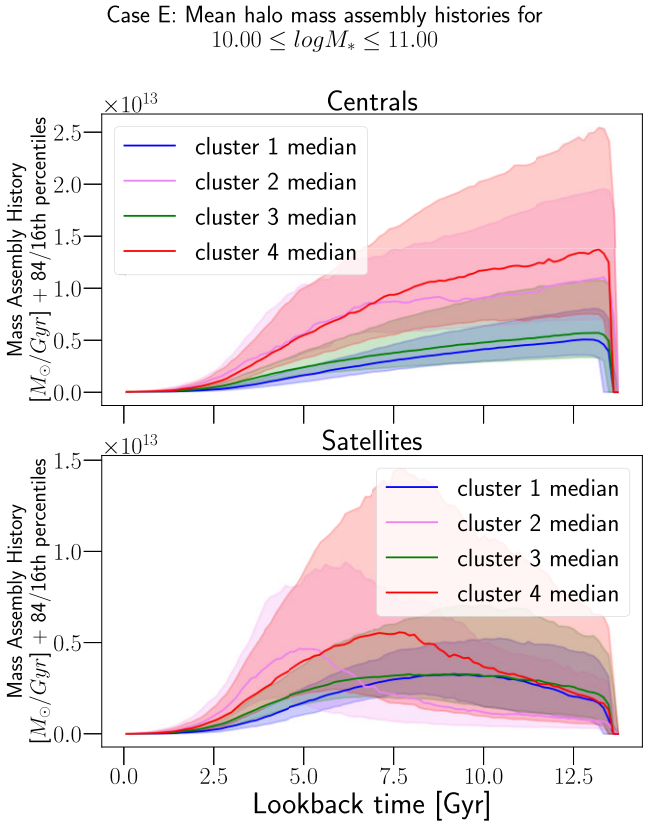

Figure 7. Case E: Median MAHs of the dark matter haloes of the galaxies from case E. Here, we find that like all other cases, the greatest differences can be seen in the halo MAH of the satellite galaxies of a given cluster, rather than their centrals. In fixing for stellar mass, we find that the satellites in cluster 2 have the most recent peak in their assembly history around 5 Gyr ago, cluster 4 has a peak around 8 Gyr ago, and clusters 1 and 3 have overlapping peaks around 10–11 Gyr ago. A point of contrast is comparing these recent peaks in the median MAH with the SFHs in Fig. 9, which are indicator of the role this growth in the halo plays in the stellar evolution. We explore this in detail in Section 5.

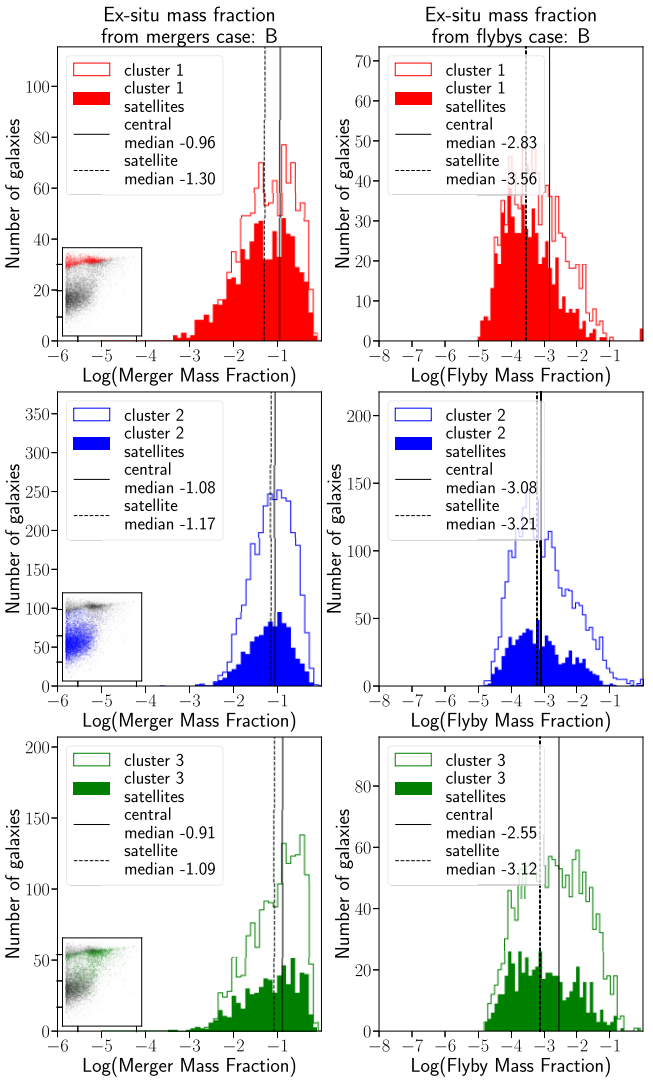

Figure 8. Case B: Distribution of *ex-situ* mass fraction from mergers (left column) and flyby events/ongoing mergers (right column) from IllustrisTNG-100 galaxies, split by cluster membership. Both the centrals and satellites in quiescent populations like clusters 1 and 3 for case B have very distinct peaks in the merger mass fraction and flyby/ongoing merger mass fraction distributions, which are distinct between centrals and satellites. Notably, it seems that galaxies in cluster 3 of case B, especially central galaxies, are likely to source an order of magnitude or more of their *ex-situ* mass fraction from mergers than galaxies in the other sub-populations. Considering this in conjunction with the mean SFHs of Fig. 5, this suggests the role mergers might play in the rate of quenching of these galaxies. While these distributions do shift when fixing for mass, the distributions are still distinct.

By contrast, a blue cloud population has significantly younger stars than its halo's mass-weighted age, indicative of the opposite. Given there is also a distinct lack of overlap between the two quenched populations (clusters 1 and 3), per Fig. 9, it is interesting that these populations have galaxies peaking at similar times of their SFH, but quenching across a wide range of time-scales.

When we end up increasing the number of clusters to 4, we found that this new population ends up selecting for galaxies that are relatively lower in mass, but are very extinct, and very much dominated by satellites.

As in the other populations, the mass-weighted age of the halo is older than the stellar matter. In the high *ex-situ* mass fraction population, this amounts to ages of $8.68^{+0.71}_{-0.70}$ and $8.27^{+1.19}_{-1.15}$ Gyr, ages that practically overlap, indicating that these mergers would play a role in star formation and evolution.

In focusing on the non-observable quantities, we find the distribution of satellite galaxies in these two populations to be of interest, as the older population (cluster 1) is distinctly dominated by satellites, and has a smaller flyby and merger *ex-situ* fraction than cluster 3, which is split more evenly in terms of their central/satellite demographics. This demonstrates that the addition of a single cluster reveals interesting populations with characteristic features, namely the sheer diversity of quiescent galaxies, possibly linked with different evolutionary histories. This is discussed in Section 5.

4.3 Colour-based clusters – case A

In case A, we cluster based on optical colour only and consider three clusters. We found that while there were superficial differences seen in the colour–mass diagram (Fig. 4), these did not extend to differences in the stellar evolution or, more importantly, the *ex-situ* mass fractions and the MAH. The metallicity histories, unlike the SFHs, overlap significantly. The *ex-situ* merger mass fraction medians between the blue cloud of cluster 2 and the green valley of

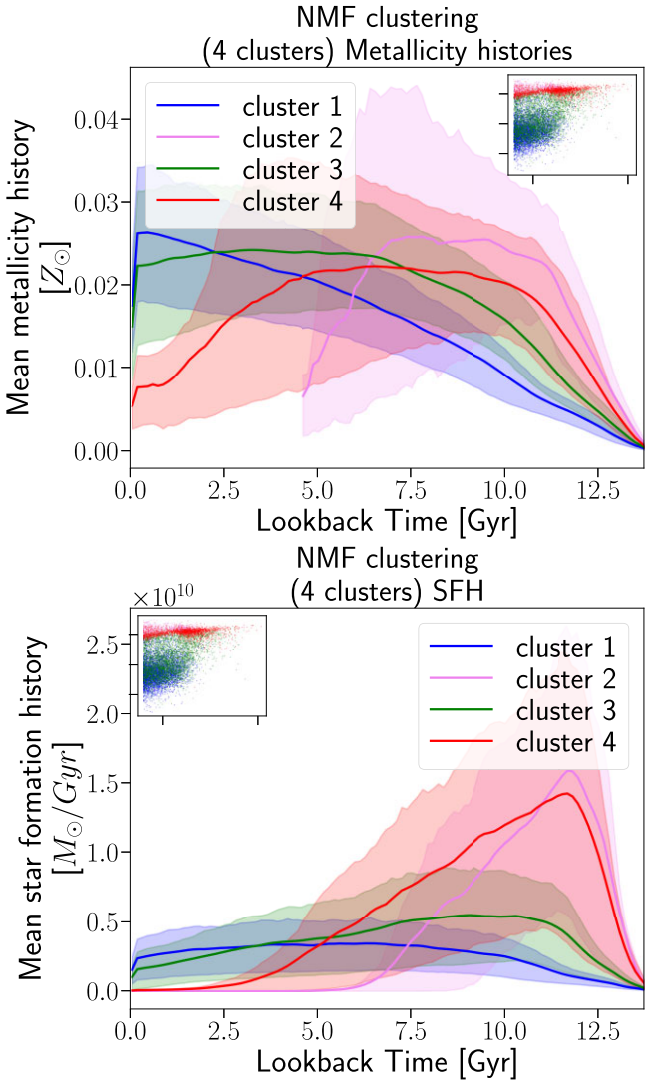

Figure 9. **Case E:** Plot of mean SFH and metallicity histories with 1σ regions shaded in, with clusters generated using smoothed NMF components of the star formation and metallicity histories. The ensuing populations are distinct in terms of both metallicity histories and SFHs. The most striking feature is the split of these means: three out of the four populations are at some stage of quenching, with two of them having decisively quenched (clusters 2 and 4).

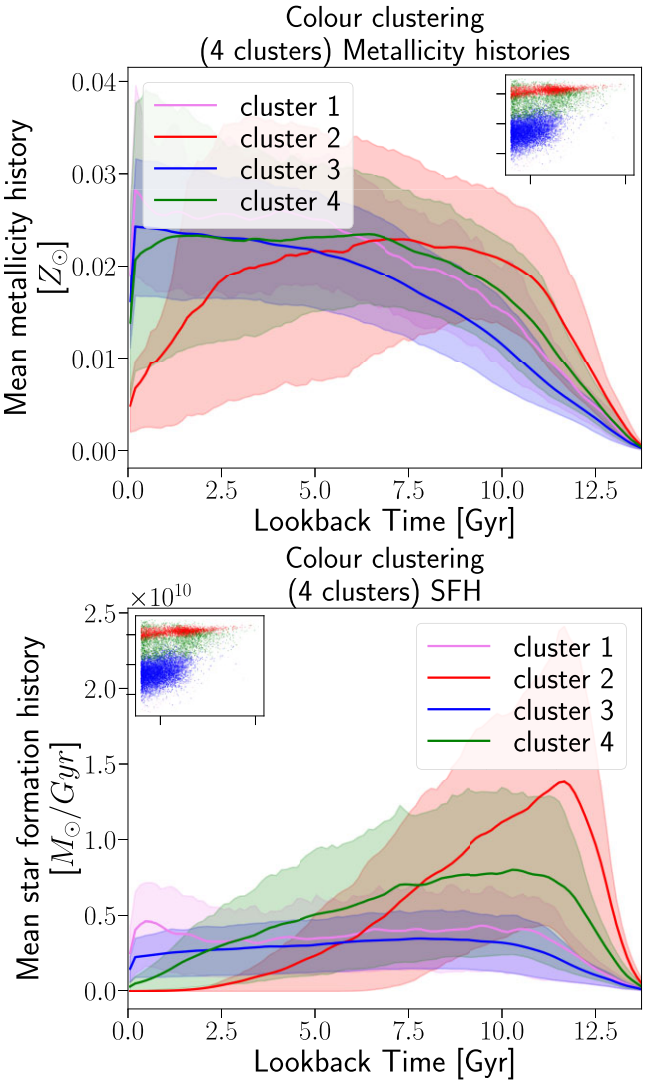

Figure 10. **Case D:** Plot of mean SFH and metallicity histories with 1σ regions shaded in, with clusters generated using photometric colours. The ensuing populations are not as distinct as in other cases discussed (e.g. Figs 5–9), but special attention should be paid to cluster 1's late evolution in the last few Gyr. As we argue in Section 5, this could serve as a shorthand for identifying post-starburst galaxies. These galaxies possess: an interesting evolutionary history, as evidenced by its *ex-situ* mass fractions.

cluster 3 are −1.06 and −1.11 versus −1.09 and −1.21 for central and satellite sub-population, respectively, and −3.02 and −3.18 versus −2.99, −3.20 for flyby mass fractions. The overall distributions are very similar as well, underscoring that these populations are not really as distinct as the rest. This distinction criterion is ultimately qualitative.

In contrast to the populations discussed in the previous subsections, here we highlight the limitations in distinguishing between galaxies across parameters ranging from observables (metallicity histories) to intrinsic parameters (dark matter halo MAH and merger histories).

4.4 Colour-based clusters – case D

In case D, we cluster based on optical colour only, but now consider four clusters. The mean star formation and metallicity histories of each cluster are shown in Fig. 10.

While clustering with only photometric colours does not really allow us to uncover much about the dark matter halo's evolutionary history, the four-cluster case produced novel populations with distinct features that are worth examining in an observational context. In the discussion we will opine on some possible characteristics, but here we will summarize the key attributes. The clusters in this case are very similar to those of case A, with a star-forming population, a quiescent one, and a population that inhabits in between (green valley). The added caveat is that the last population incorporates some lower mass and redder galaxies, and that the last cluster (cluster 3) incorporates a subset of galaxies from the 'blue cloud'. What is apparent with cluster 1's galaxies is that while these galaxies at fixed masses have similar star formation and metallicity histories, they tend to slightly exceed cluster 3's average in SFH and metallicity history in the last 2 Gyr (Fig. 10). Their *ex-situ* mass fraction distribution is unique in that the merger mass fraction has a similar median as cluster 1, but

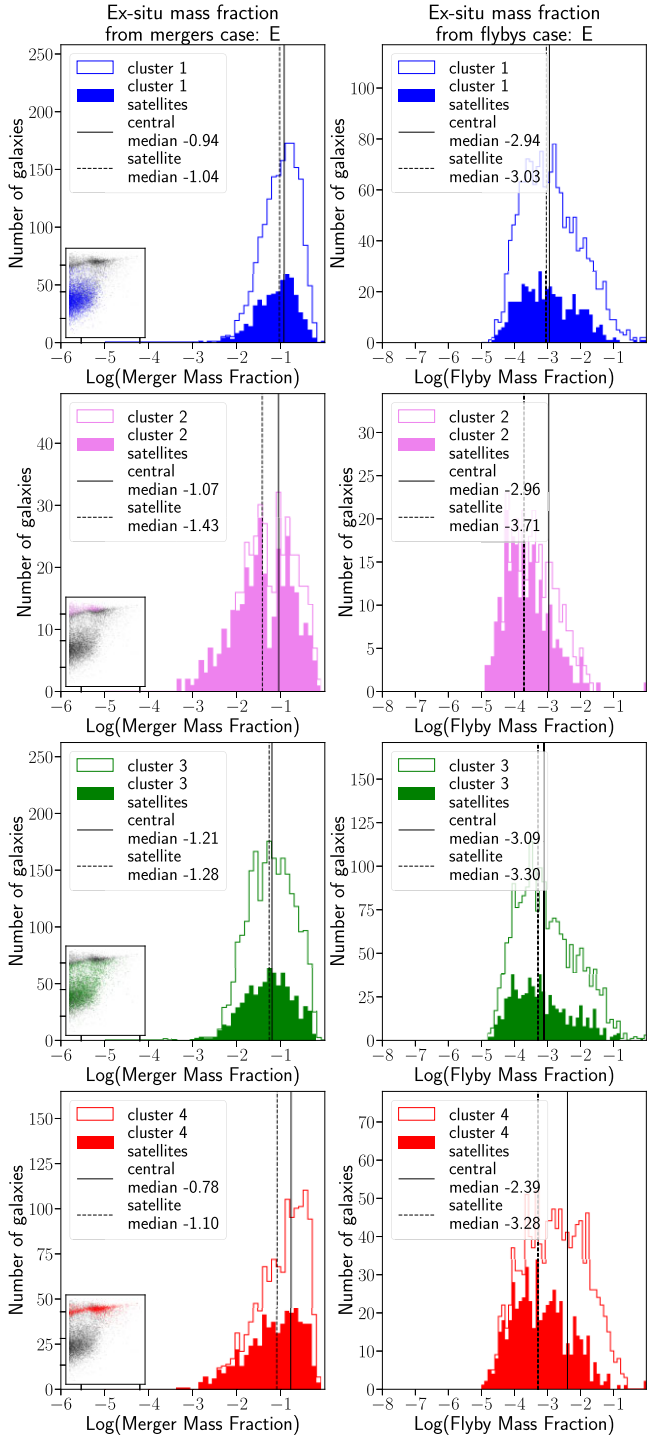

Figure 11. Case E: Distribution of log *ex-situ* mass fraction from mergers $f_{\rm M}$ (left column) and flyby events $f_{\rm Flyby}$ (right column) from IllustrisTNG-100 galaxies, split by cluster membership. Cluster 4 is notable in that the distribution of $f_{\rm Flyby}$ across centrals and satellites has different medians and peaks around -2 and -3, respectively – a stark contrast to other quenched populations (clusters 2 and 3), whose $f_{\rm Flyby}$ is not as decoupled. This indicates mergers might play a role in delaying quenching in cluster 4 compared to the other populations. Of interest is cluster 3, whose wide spread in the distribution of $f_{\rm M}$ might be indicative of differences in the merger history compared to other clusters. One could posit that it challenges whether or not this population is actually a green valley population, as mergers are expected to be a key component in the transition from blue to red populations.

the flyby mass fraction is considerably higher, median value of -2.45 for satellites and -3.08 for centrals, indicating that unlike any of the populations found in this clustering or cases B and E, the satellites are sourcing more of their *ex-situ* mass fraction from flybys than centrals, and the distribution is almost bimodal. This must be taken with the caveat of relatively low statistics, with only 551 galaxies total in the population and it being (67.51 per cent) satellite dominated, versus 66.30 per cent for the red sequence and 26.84 per cent for the blue cloud population. We discuss the potential this population has as a shorthand for identifying post-starburst (PSB) galaxy populations in our discussion.

4.5 Colour- and NMF-derived clusters – case C

We explored the clusters that would emerge if we combine the parameter spaces used in previous sections: NMF representations of star formation and metallicity histories alongside photometric colours. Our reasoning was twofold: to explore the overall utility of photometric colours as additional parameters, and to highlight additional sub-populations of interest.

Despite the fact that populations produced greatly resembling those found in case A in the colour–mass diagram, we find that unlike case A, these populations have distinct metallicity and SFHs – demonstrating that the clustering adroitly differentiates between different star formation and metallicity history profiles. Notably, the green valley population (cluster 3) quenches along a distinct timescale compared to the redder galaxies of cluster 2 (starts quenching around 1 Gyr lookback time versus 6.5 Gyr lookback time). This distinction is also readily apparent in the metallicity history, which has each population peaking at different times for its metallicity history, demonstrating the diversity of each population's chemical enrichment. We can also extend this analysis to non-observable parameters, which were a source of contention in using the clusters produced by case A. For the *ex-situ* mass fractions, we find that the addition of NMF components to our colour clusters does noticeably alter the composition. However, these changes do still come with some of the issues initially raised. The largest change is seen in the distributions of the flyby and merger mass fractions of galaxies in the green valley, cluster 3.

Here, we find that the two-sided KS test gives its only significance ($p > 0.05$), with a $p = 0.2$ for overlap between clusters 2 and 3. This underscores existing doubts we had about this population, as it shows that there is a significant probability of these two populations being the same. The decision regarding distinct populations is ultimately qualitative, but we use this as grounds to favour case B over case C as being a much more distinct population, which is the ultimate goal of this paper: distinct populations.

4.6 Colour- and NMF-derived clusters – case F

For the final case, we explore the addition of a fourth cluster to the parameter space used in case C.

We find that this new cluster produces a population that is extremely satellite dominated, and occupies a low mass, but very quiescent branch of the red sequence. This is underscored by the distinctly sharp peaks in its star formation and metallicity history, and rapid quenching of this population, with its mean having quenched by 6–7 Gyr lookback time.

We find that clusters 2 and 3 have strongly overlapping medians for their *ex-situ* merger mass fractions (-0.82, -1.12 for centrals and satellites versus -0.99 and -1.21), with the overall distribution of flyby mass fractions between the two populations being similar.

For cluster 3, the distribution of log flyby mass fraction is overall bimodal, as in case C with peaks at approximately −3.5 and −1.5. There is a larger proportion of central galaxies at lower merger mass fractions than in the red sequence population, indicative of a broader distribution. Compared to case E, clusters 2 and 3 are qualitatively too similar.

5 DISCUSSION

5.1 The effectiveness of using photometric colours versus NMF

While SFHs are an important marker of stellar and baryonic evolution within galaxies, as we show, they do not tell us everything. Cases A and D demonstrate the failure of colour-based clusters to produce a clear distinction beyond the SFHs. Examining the mean SFHs reveals an overlap between populations, and looking at the mass-weighted ages of the stellar and halo components, we find for case A, stellar mass-weighted ages of $9.48^{+1.41}_{-1.32}$, $6.24^{+0.87}_{-0.84}$, and $7.01^{+1.01}_{-0.97}$ Gyr for each of its clusters, and mass-weighted mean metallicities of $0.021^{+0.0022}_{-0.0027}$, $0.017^{+0.0022}_{-0.0024}$, and $0.019^{+0.0016}_{-0.0021}$ $Z_\odot$. Similarly for case D: $6.08^{+1.19}_{-1.06}$, $9.55^{+1.34}_{-1.27}$, $7.01^{+0.86}_{-0.84}$, and $7.72^{+1.08}_{-1.10}$ Gyr for each of its clusters, and mass-weighted mean metallicities of $0.022^{+0.0011}_{-0.0046}$, $0.020^{+0.0022}_{-0.0023}$, $0.017^{+0.0024}_{-0.0025}$, and $0.020^{+0.0018}_{-0.0030}$ $Z_\odot$.

When we consider non-observables, we consistently see overlap in the *ex-situ* mass fractions and median MAHs in the photometry-only clusters, further reinforcing that the divisions produced here do not capture the differences in evolutionary histories we are looking for and find in other clusters. Particularly, looking at the *ex-situ* mass fraction for case A, between clusters 2 and 3, we find that the overall distributions for both of these populations peak at very similar log mass fractions, with overlapping medians for flyby and merger mass fractions (−1.06, −1.11 versus –1.09 and –1.21 for mergers, −3.02 and −3.18 versus −2.99 and −3.20 for flybys). This is even more pronounced in case D, where clusters 1 and 3 have overlapping merger mass fractions, with overlapping medians for both the centrals and satellites in these populations (−0.88 and −1.20 for cluster 1, –0.83 and –1.18 for cluster 3).

One population that is of lingering interest, and that we address later, is cluster 1 of case D. This is a sub-population of galaxies whose SFH and position on the $M_* - (G - R)$ colour plot greatly resemble those of the 'blue cloud' galaxies identified in cluster 2, but is a satellite-dominated population, with a significantly larger *ex-situ* mass fraction from flybys than cluster 2, particularly from its satellites (median value of −2.45 versus −3.27). In addition, the mean star formation and metallicity histories for this population exhibit a notable peak in the last 2 Gyr of lookback time – indicative of the presence of stars of that age. This population is exclusive to this clustering (four clusters, using broad-band colours only). Partly, this will be driven by the fact that our NMF basis does not have the resolution at young ages to reliably pick up this population. Colours, on the other hand, are particularly sensitive to the SFH in the last Gyr (Chaves-Montero & Hearin 2020), and can be combined effectively to identify PSB galaxies (Wild et al. 2014). The sensitivity of optical broad-band colours to recent star formation combined with the heavy compression of SFHs into four NMF basis (with poor resolution at late times) likely explains why we can pick up this population more easily in case D. As we discuss later, this population can be linked to PSB galaxies identified elsewhere in the literature.

In contrast to these cases, cases B and E host significant differences in their mean star formation and metallicity histories (see Figs 5 and 9). This also manifests in the mass-weighted ages of the stellar and halo components: $9.91^{+1.26}_{-1.21}$ Gyr for cluster 1, $6.26^{+0.82}_{-0.78}$ Gyr for cluster 2, and $8.27^{+1.19}_{-1.15}$ Gyr for cluster 3, and $7.68^{+1.45}_{-1.33}$ Gyr for cluster 1, $9.09^{+0.64}_{-0.55}$ Gyr for cluster 2, and $8.88^{+0.70}_{-0.72}$ Gyr for cluster 3 of case B, respectively; and $5.81^{+0.65}_{-0.63}$ Gyr for cluster 1, $10.59^{+0.92}_{-0.86}$ Gyr for cluster 2, $7.22^{+0.76}_{-0.75}$ Gyr for cluster 3, and $9.32^{+1.22}_{-1.09}$ Gyr for cluster 4. and $9.19^{+0.65}_{-0.53}$ Gyr for cluster 1, $7.08^{+0.70}_{-0.72}$ Gyr for cluster 2, $8.93^{+0.57}_{-0.57}$ Gyr for cluster 3, and $8.48^{+0.97}_{-1.12}$ Gyr for cluster 4 of case E, respectively. Note how the satellite-dominated population of cluster 1 has, on average, a younger halo than its stars. This is the first of many indicators about how the differences uncovered extend beyond the parameters we clustered.

5.2 Analysing non-observables to distinguish between evolutionary histories

Non-observable parameters, such as the merger history, dark matter halo MAH, *ex-situ* mass fractions, and mean mass-weighted ages, reveals important information regarding the demographics of galaxies in the populations of the cases we identified, and how they behave.

In this section, we will focus on analysing in detail the populations revealed in cases B and E. The results with colour clustering (cases A and D) have shown while clustering with photometric colours does yield some superficial differences in the populations identified, the most interesting were found with clusterings that made use of star formation and metallicity histories. Our preference of cases B and E over cases C and F stems from case C having one population where it had a significant ($p > 0.05$) p-value from a two-sided KS test, meaning that the distributions studied (*ex-situ* merger mass fraction) of two populations had a very high probability of being similar.

The populations identified in cases B and E are distinct and highlight how the existence of a green valley is not that well supported, as splitting along the red sequence, roughly based on the central–satellite status of a galaxy, reveals much more substantial information about its evolutionary history, as corroborated by significant differences in the *ex-situ* mass fraction (mergers) and MAH.

5.2.1 *Case B: three cluster populations*

Case B results in a single star-forming population identified, cluster 2, the remaining two splitting along the red sequence. When we keep stellar mass fixed, we find significant differences in their mean SFHs and metallicity histories. Specifically, while both peak at a similar time, the time it takes for the mean SFH to drop to zero differs greatly (Fig. 5). This is supported by a difference seen in the MAH and *ex-situ* mass fractions – where the redder, more satellite-dominated population (78.96 per cent) of cluster 1 has a similar distribution of *ex-situ* mass fraction between centrals and satellites, cluster 3, the higher mass end of the red sequence, has centrals with a higher *ex-situ* mass fraction, its distribution peaking at a larger fraction (Fig. 8). This indicates that these centrals are sourcing a greater proportion of their *ex-situ* mass from mergers and that mergers in cluster 3 seem to allow star formation to continue for so long compared to galaxies of a similar mass in cluster 1.

The median MAHs complicate this picture, particularly when comparing the satellite sub-population, which seem to have a 'late peak', coinciding at around 6 Gyr ago for cluster 1, 8–9 Gyr for cluster 3 (Fig. 6). This means that a major change happened in cluster 1, often after star formation stopped, whereas in cluster 3, this seems to have preceded quenching. The halo's mass-weighted age is $7.68^{+1.45}_{-1.33}$ Gyr, the stellar mass-weighted age is $9.91^{+1.25}_{-1.20}$ Gyr in cluster 1 versus $8.88^{+0.70}_{-0.71}$ and $8.27^{+1.19}_{-1.15}$ Gyr, respectively, for cluster 3. This signals that most of the stellar mass formed long before the halo gained all

its mass. This is contrary to other populations and, when contrasted with cluster 3, seems to indicate how mergers might have allowed the quenching to be delayed and forestalled with mergers or how mergers brought in gas or younger stellar populations. So clearly, the satellite-dominated case has older stars on average than the halo it inhabits, but centrally dominated populations do not. The blue cloud population has a larger gap in its age, like cluster 1, but cluster 3, despite inhabiting the red sequence like cluster 1, has an overlapping range of ages, with the stars being a little younger than the halo.

This could corroborate the peak seen in the MAH of cluster 1 (Fig. 6) but raises significant questions about the merger history of these populations, which could be explored in a later work.

5.2.2 *Case E: four cluster population*

In case E, we aimed to explore how the clustering changes when we re-cluster the population and allow for four populations instead of three.

Interesting information can be gleaned when we examine indicators of the halo's evolution and merger histories. The median MAHs of these satellite galaxies of these three populations (clusters 2, 3, and 4) peak at 5, 9, and 8 Gyr ago in lookback time, approximately. By 5 Gyr ago, cluster 2 is almost entirely quenched, making it appear to be a more exaggerated version of cluster 1 from case B – satellite dominated, visible shift in halo assembly history after quenching. Meanwhile, the peak in the other two suggests that much like what was discussed in case B, something is a bit different with satellite galaxies here.

Extending to *ex-situ* mass fractions, we find that cluster 4 is the population with a distribution of *ex-situ* mass fraction that is significantly greater than the rest, both in overall distribution and in its merger mass fraction medians (-1.10 and -0.78 for satellite and central). What is even more notable is the order of magnitude difference seen in *ex-situ* mass fractions of clusters 2 and 4 from flybys, between centrals and satellites, with centrals in both cases having a distribution peaking at a higher mass fraction than satellites. This indicates that the centrals in both cases are evolving slightly differently when compared to cluster 3. Mergers clearly play a critical role in these populations. With such a critical difference seen in the flyby fraction for cluster 4 compared to the rest, this seems to indicate that the quenched galaxies here are possibly undergoing more significant interactions. This further motivates additional exploration of the merger histories of these populations in a future paper.

Examining the mass-weighted ages of the stellar and halo components reveals a similar pattern as in case B: the redder and the more satellite dominated, the younger the halo is with respect to the stellar component ($7.08^{+1.80}_{-1.30}$ Gyr versus $10.60^{+0.92}_{-0.86}$ Gyr for cluster 2, $8.48^{+0.97}_{-1.12}$ Gyr versus $9.33^{+1.22}_{-1.09}$ Gyr for cluster 4 and $8.93^{+0.57}_{-0.57}$ Gyr versus $7.22^{+0.76}_{-0.78}$ Gyr for cluster 3). Interestingly, even though cluster 2 is much more quenched, since it is largely satellite dominated, its mass-weighted age for the halo is lower than that for cluster 4, which is more closely dominated by centrals. In addition, the stars in cluster 2 are older than those in cluster 4. This further motivates the need of a detailed study of the merger histories of these galaxies. However, we have already shown how this clustering is an effective proxy for extracting populations with very distinct features, for both the stellar and halo components.

Regarding the relationship between case E's clusters and case B's clusters, we examined the overlap fraction of these populations: What percentage of galaxies in a particular cluster for case E came from a particular cluster in case B. We found that >99 per cent of galaxies in cluster 1 in case E came from cluster 2 in case B, and in cluster 2 of case E 99 per cent of galaxies came from cluster 1 in case B, and an additional 1 per cent from cluster 3. Cluster 3 sourced 63 per cent from cluster 2 and 37 per cent from cluster 3. For cluster 4, it sourced 49 per cent from cluster 1 and 51 per cent from cluster 3. This highlights that the galaxies identified in cluster 1, the very quenched population, were a mostly satellite subset identified in case B's clustering.

It is worth noting that for future works, the implementation of normalization is particularly important. We normalized the smoothed SFHs with a max-abs normalization as *sklearn.prepreprocessing.normalize* allows you to choose which axis to normalize along, whereas its scaler object implementation does not for the maximum absolute value scaling. Normalizing each SFH between 0 and 1 produced the results here. With the scaler object, it does not. This aligns with earlier caveats that clustering can produce unstable populations, so it is worth noting that the extremely quenched population is liable to change under the implementation of a specific normalization used.

5.3 Links with known populations

The largest takeaway is that the clustering is effective at identifying and navigating sub-population of the red sequence, and isolating populations with a relatively unique set of formation histories. What is notable is the split in the red sequence of quiescent galaxies seems to be largely driven by the central/satellite status, and their *ex-situ* merger mass fraction, as demonstrated in case B, which explored populations produced from clustering NMF components of the star formation and metallicity histories of IllustrisTNG galaxies, into three selected populations. These populations are defined by a split between star-forming and quiescent galaxies (cluster 2 versus clusters 1 and 3), and an additional split between the satellite-dominated quiescent population of cluster 1 and the upper mass branch of the red sequence, cluster 3, characterized by its large *ex-situ* merger mass fraction (Figs 5 and 8). Cluster 1 is a population whose largest event for its dark matter haloes occurs around 5–6 Gyr ago, with significant growth in the halo mass seen in the satellite galaxies of this satellite-dominated population, largely after the population has begun to quench. By contrast, cluster 3, the more centrally dominated quiescent population, is characterized by a more gradual reduction in its SFH, potentially indicative of the role major mergers might play in shaping the rate at which these galaxies might quench, as described by Hani et al. (2020) and Quai et al. (2021).

Expanding the number of clusters for the same parameter space as above to 4 (case E), we find a parallel to the work of Hani et al. (2020) and Quai et al. (2021) regarding the role of SFHs and mergers, where for star-forming galaxies, major mergers tend to have a significant impact in increasing the star formation rate in the period following a merger, albeit with the possibility of further hastening any quenching that might follow compared to their control group. This higher merger mass fraction might place a constraint on the local environment of these galaxies, as Oh et al. (2019) find for clusters of galaxies, where only recently accreted galaxies show observational evidence of merger-induced changes. For the former, satellite-dominated quiescent population, similarities can be seen with Donnari et al. (2020) and Oh et al. (2019), where pre-processing and infall can help account for the quenching of these galaxies.

Little differentiation emerges within the blue cloud population, and instead we get three populations at three different stages of quenching. Comparing the mean SFHs, we note a significant split across clusters 2, 3, and 4. While cluster 3 could be classified as a population

that is not fully quenched, the quenching time-scale between clusters 2 and 4 can be clearly seen in Fig. 9. Cluster 2's mean star formation seems to quench from 6 to 9 Gyr ago, whereas that of cluster 4 starts quench around 2–5 Gyr ago. This older population is significantly dominated by satellites (87.95 per cent for cluster 2, versus 55.27 per cent for cluster 4 and 37.24 per cent for cluster 3), indicating that cluster 2 is a population that is truly red and dead, and primarily satellite. Of note is how the key discriminants of a given galaxy in Donnari et al.'s (2020) work produce populations that align with ours: whether it quenched before infalling as a satellite, or following an infall event whose 16/84th percentile intervals for the SFHs of cases B and E resemble periods when different populations of satellites quenching at different times in Donnari et al. (2020; see Figs 5 and 9).

In cases E and F, the addition of a fourth cluster reveals an extremely quenched, satellite-dominated population inhabiting the red sequence. By contrast, doing so for the colour-based clusters, i.e. case D, reveals an interesting subset of the 'blue cloud' population of star-forming galaxies.

In addition to a late peak in the star formation and metallicity histories in Fig. 10, a few more features of this population stand out to reinforce this picture: we find that satellites in cluster 1 have a significantly larger *ex-situ* mass fraction from flybys (median: −2.45 for satellites and −3.08 for centrals, versus medians of −3.09 for centrals and −3.27 for satellites in cluster 3) than the blue cluster, and that unlike any other population, the *ex-situ* fraction is larger for the satellite sub-population than centrals. These *ex-situ* fractions are remarkably similar to the green valley population of cluster 4 (−2.58, −3.09 central and satellite medians).

Looking at the halo and stellar mass-weighted ages, we find that cluster 1 has a mean halo mass-weighted age of $8.34^{+1.25}_{-0.44}$ and $6.07^{+1.19}_{-1.06}$ Gyr for the mean stellar mass-weighted age, very similar to cluster 3's $9.17^{+0.55}_{-0.46}$ and $6.36^{+0.86}_{-0.84}$ Gyr, respectively. Altogether, this paints the picture of this population being an interesting approximation of a PSB galaxy: a galaxy where its star formation has just ceased, and is about to transition onto the red sequence, potentially with the *ex-situ* mass fraction information being a key indicator of the role of mergers in this transition. Given that this population was found using photometric colours, it demonstrates the potential of this method even in surveys where we would have no access to star formation and metallicity histories (see Wild et al. 2014).

Clusters such as cluster 3 in case B and cluster 3 in case E, with galaxies that inhabit the red sequence but have a larger *ex-situ* merger fraction than others, have been seemingly able to extend their star-forming epoch as a consequence of these mergers, either through shocking existing gas or through possible pre-processing and infall of neighbouring galaxies (Donnari et al. 2020). In either case, this link between mergers and delayed quenching is of interest, and additional works in the literature support the link between major mergers and their role in driving and suppressing star formation in these galaxies. Since this work is not primarily focused on merger histories, and rather just identifying distinct evolutionary histories, we present this topic as an area of interest for a follow-up investigation.

5.4 Areas of future work

The absence of a 'green valley' population is notable, as the clustering largely divides galaxies that might be considered green valley (i.e. those seen in case A) between clusters 1 and 3. The slow quenching of cluster 3 bears a notable similarity to the quenching described by Schawinski et al. (2014) of quiescent galaxies. Moreover, the split evolutionary tracks identified in Trayford et al. (2016) draw an interesting parallel as well to the variety of quenched populations found in cases B and E. Exploring the way these populations manifest in non-optical wavelengths would also be an area of interest, building upon the criticisms of the green valley presented by Eales et al. (2018).

Pertinent questions are raised in works like Weigel et al. (2017), Zinger et al. (2020), Pawlik et al. (2019), and Wilkinson, Pimbblet & Stott (2017), among others, such as the relevance of major mergers in driving the evolution of these galaxies and the role AGNs might play in regulating the dispersal of gas in these galaxies. Of particular interest is Donnari et al.'s (2020) series of papers, which explored the role of pre-processing, and would serve as an effective and direct test of the ability of these sub-populations in replicating the results of simulation-based work using only 'observable' parameters. In particular, points (i)–(iii) of Donnari et al.'s (2020) conclusion bear a striking resemblance to the sub-populations of galaxies we have described in cases B and E: that of lower mass, satellite-dominated populations that are largely quenched, with an associated accretion time of 4–6 Gyr, possibly linked to an infall event, with the exception of bluer galaxies. They also identified galaxies along the upper mass range of the red sequence, where above $\log M_*/\mathrm{M}_\odot = 10$, the satellite population is largely quenched, further highlighting the similarities of those satellites and the satellite-dominated sub-population from case B. Finally, to quote Donnari et al. (2020): 'While, as expected, the quenched fractions of IllustrisTNG central and satellite galaxies are generally lower at higher redshifts (Fig. 2), frequent manifestations of environmental processes in hosts more massive than about 10^{13} $\mathrm{M}_\odot$ are already in place at $z \sim 1$ and the bulk of the $z = 0$ group and cluster quenched satellites ceased their star formation many billion years ago: 6–10, 1–7, and 4–8 Gyr ago (16th–84th percentiles) for satellites that quenched as centrals, in their current host, or as satellites before falling into it, respectively'. This describes populations that greatly resemble our own yet again; the population quenching at 1–7 Gyr ago resembles that of cluster 3 in case B: a central-dominated host population, whereas the 6–10 and 4–8 Gyr ago intervals resemble cluster 1 in case B, or they can be further delineated when applying these intervals to case E.

Their work's conclusion is in tandem with one of our own: that satellite galaxies have a diverse range of paths to quenching, and for us, in several different clusterings, that diversity is captured by some of our clusters.

We have only briefly touched upon the merger histories of these clusters, and would encourage the reader to consider exploring some of the questions regarding the histories presented by these clusters. In particular, how closely do the identified sub-populations correlate with differences in environment? This is relevant given some identified links between environment and the number of associated mergers, especially for more massive galaxies (e.g. Yoon, Im & Kim 2017), which highlights how below masses of $\log M_*/\mathrm{M}_\odot \geq 11.0$ the number of mergers a given galaxy experiences ceases to correlate with local density. The application of these populations, when cross-referenced with environmental data from TNG-100, could help provide insights as to the extent these clusters might trace out the environmental dependence of these populations.

Moreover, as we discussed in an earlier section, we have also traced out a testable shorthand for identifying potential PSB galaxies and generating broad predictions about their non-observable properties just from using photometric colours in our clustering. This population

is satellite dominated, with a large *ex-situ* mass fraction. We will explore the link between traditional PSB galaxies and this population in a follow-up paper.

6 CONCLUSION

We extracted a series of 'observable' parameters from the IllustrisTNG-100 simulation, and clustered them with a GMM, studying a variety of parametrizations with different clusters. We focused on clustering with the photometric colours $u - g$, $g - r$, $r - i$, and NMF representations of the extracted star formation and metallicity histories. We ultimately found that in terms of effectively identifying populations with distinct evolutionary histories, the use of the star formation and metallicity histories was indispensable. Using these parameters in our clustering produced clusters with distinct histories associated with the dark matter haloes of these galaxies. In particular, we found that cases B and E produced the most distinct of these evolutionary histories, as seen in Section 5 and Figs 5, 6, 8, and 9.

We highlight case B as the most significant sub-population of interest in this analysis, owing to distinct splits seen in the SFHs and metallicity of the populations, this distinction extended to differences found in the halo and evolutionary components, i.e. the *ex-situ* mass fractions, the MAH, and the mass-weighted ages of the stellar and halo components. The most consequential split found in this three-cluster case is between the populations that inhabit the red sequence: a lower mass, satellite-dominated one, and a higher mass central-dominated one. Taking what was discussed in Section 5 we concluded that they had significantly different evolutionary histories.

Case E is interesting owing to the distinct populations it identifies primarily within the red sequence, and as an examplar of how adding an extra cluster to our algorithm alters the populations initially discussed in case B. We found three populations at varying degrees of quenching, and a single star-forming population. Two of these populations, clusters 2 and 4 are definitively quenched, and within distinct windows of time. The earlier it quenched, the more satellite dominated the population is. Interestingly, when comparing the mean mass-weighted ages of the stellar and halo mass, these two populations have older stellar mass-weighted ages than the halo mass-weighted ages, whereas the opposite is true for the other two populations. This is indicative of a major difference in the role mergers play in the evolution of these populations.

Case D, while producing populations not as distinct as those in cases B and E, is notable in what we found in cluster 1, a population that could be potentially described as related to PSB galaxies, given the spike in its star formation and metallicity histories, and we only needed photometric colours to identify it, and has some unique features in its *ex-situ* mass fraction and recent stellar evolutionary history.

We summarize the key conclusions below:

(i) The cases that made use of the star formation and metallicity histories in their clustering produced results that had notable differences in the distribution of the *in*/*ex-situ* mass fraction, merger history, and halo mass assembly history, indicative of the depth of the differences between clusters.

(ii) The populations identified in cases B, C, E, and F also echo a point raised elsewhere in the literature, where satellite galaxies in particular seem to follow a diverse range of pathways to quenching in the present day, and that these pathways are reflected by the sub-population identified in case E, and cases B and C to a lesser extent: as the 84/16th percentile intervals given by Donnari et al. (2020) closely resemble those seen for the quiescent populations of case E. This also suggests the link between infall and the populations identified by these clusters.

(iii) The populations identified by our clustering show that the red sequence of quiescent galaxies is split into a central-dominated sub-population and a satellite-dominated one. The satellite-dominated one can be further split if we examine these populations with four clusters instead of three (i.e. case E), with differences between the mass-weighted ages of the halo and stellar component hinting at different modes of quenching.

(iv) While colour-based clusterings did not produce populations that were as distinct as those in cases B, C, E, and F, there are still populations of interest, namely case D, cluster 1, where clustering with broad-band photometric colours for four populations produces a subset of star-forming galaxies that are of potential observational interest. This cluster, cluster 1, is a subset of the star-forming 'blue cloud' population, but with relatively recent spike in its star formation and metallicity history (Fig. 10), and with considerable differences in its *ex-situ* mass fraction that could suggest a merger/flyby-rich subset of galaxies in the blue cloud. We argue that this population bears some notable similarities to PSB galaxies that have been found elsewhere in the literature, their precise relationship with PSB galaxies needs to be characterized.

(v) Our clusterings in cases B and E underscore that the most important and distinct divisions of galaxies do not necessarily reproduce a green valley population as identified elsewhere in the literature, rather it shows that the red sequence is an incredibly diverse population with a variety of evolutionary histories giving rise to those galaxies.

We have identified a number of populations that are of interest for future work, in the context of other cosmological hydrodynamic simulations, where the populations we identified can be compared to the carefully selected ones seen in the literature (e.g. Wilkinson et al. 2017; Hani et al. 2020; Quai et al. 2021), or they can be extended into an observational context, testing the general predictive power of these populations, and the simulation they were calibrated on, and juxtaposed with existing work that has attempted to do so (Donnari et al. 2020).

This work has demonstrated that the incorporation of quantities such as the star formation and metallicity histories of galaxies provides valuable insight into their evolutionary histories that exceeds what could be found using photometric colours. While these clusterings are not necessarily the best possible divisions of galaxies by evolutionary histories, they do have some distinct features that are of interest. The utility provided by these SFHs and metallicity histories also underscores that the effort to extract those histories is not wasted, and that with these full histories of star formation and chemical enrichment, they can be leveraged to explore the evolutionary histories of these galaxies. Of course, it remains to be seen how an analysis on real data compares to the clusters we find here. We leave a detailed comparison between data and different cosmological simulations for a future paper.

ACKNOWLEDGEMENTS

The authors would like to thank the referee for a thoughtful report that led to visible improvements in this paper and also Dr Jonas Chaves-Montero for their helpful feedback on SFHs and their influence on photometric colours. The authors also want to thank Dr Vivienne Wild for insightful commentary on PSB galaxies.

DATA AVAILABILITY

The data underlying this article are available on IllustrisTNG website (https://www.tng-project.org/data/docs/specifications/). Data catalogues are freely available on their website, alongside their supplementary catalogues, which we made use of in this work. The MAHs were computed by Harry Chittenden and have been submitted for publication (Chittenden & Tojeiro 2022). *sklearn* is a public python package, and was used for all the machine learning-related tasks. A notebook with the data and code summarizing the figures from this work is available at the following repository: https://github.com/tsfraser/FraserTojeiroChittendenPaper.

REFERENCES

Bertone S., Conselice C. J., 2009, MNRAS, 396, 2345
Bundy K., Fukugita M., Ellis R. S., Targett T. A., Belli S., Kodama T., 2009, ApJ, 697, 1369
Caliński T., Harabasz J., 1974, Commun. Stat. Theor. Methods, 3, 1
Carnall A. C., McLure R. J., Dunlop J. S., Davé R., 2018, MNRAS, 480, 4379
Chaves-Montero J., Hearin A., 2020, MNRAS, 495, 2088
Chaves-Montero J., Hearin A., 2021, MNRAS, 506, 2373
Chen Y., Mo H., Li C., Wang H., Yang X., Zhang Y., Wang K., 2020, ApJ, 899, 81
Chittenden H. G., Tojeiro R., 2022, MNRAS, 518, 5670
Cochrane R., Best P., 2018, MNRAS, 480, 864
Cohn J., 2018, MNRAS, 478, 2291
Cole S., Lacey C. G., Baugh C. M., Frenk C. S., 2000, MNRAS, 319, 168
Davé R., Anglés-Alcázar D., Narayanan D., Li Q., Rafieferantsoa M. H., Appleby S., 2019, MNRAS, 486, 2827
Davies D. L., Bouldin D. W., 1979, IEEE Trans. Pattern Anal. Mach. Intell., PAMI-1, 224
Diemer B., Sparre M., Abramson L. E., Torrey P., 2017, ApJ, 839, 26
Donnari M. et al., 2020, MNRAS, 500, 4004
Eales S. A. et al., 2018, MNRAS, 481, 1183
Guo H. et al., 2014, MNRAS, 441, 2398
Hahn C. et al., 2022, ApJ, preprint (arXiv:2202.01809)
Hani M. H., Gosain H., Ellison S. L., Patton D. R., Torrey P., 2020, MNRAS, 493, 3716
Henriques B. M. B., White S. D. M., Thomas P. A., Angulo R., Guo Q., Lemson G., Springel V., Overzier R., 2015, MNRAS, 451, 2663
Ivezić Ž., Connolly A., VanderPlas J., Gray A., 2014, Statistics, Data Mining, and Machine Learning in Astronomy: A Practical Python Guide for the Analysis of Survey Data. Princeton Series in Modern Observational Astronomy. Princeton Univ. Press, Princeton, NJ, https://books.google.ca/books?id = h2eYDwAAQBAJ
Jiang F., van den Bosch F., 2014, MNRAS, 440, 193
Lagos C. d. P. et al., 2016, MNRAS, 459, 2632
Marinacci F. et al., 2018, MNRAS, 480, 5113
Martin G., Kaviraj S., Devriendt J. E. G., Dubois Y., Pichon C., 2018, MNRAS, 480, 2266
Moulavi D., Jaskowiak P. A., Campello R. J., Zimek A., Sander J., 2014, in Proceedings of the 2014 SIAM International Conference on Data Mining. p. 839
Moustakas J. et al., 2013, ApJ, 767, 50
Naiman J. P. et al., 2018, MNRAS, 477, 1206
Nelson D. et al., 2017, MNRAS, 475, 624
Nelson D. et al., 2018, Comput. Astrophys. Cosmol., 6, 2
Nelson D. et al., 2019, Comput. Astrophys., 6, 29
Obreschkow D., Elahi P. J., Lagos C. D. P., Poulton R. J., Ludlow A. D., 2020, MNRAS, 493, 4551
Oh S. et al., 2019, MNRAS, 488, 4169
Pawlik M. M. et al., 2018, MNRAS, 477, 1708
Pawlik M., McAlpine S., Trayford J., Wild V., Bower R., Crain R., Schaller M., Schaye J., 2019, Nat. Astron., 3, 440
Pedregosa F. et al., 2011, J. Mach. Learn. Res., 12, 2825
Pillepich A. et al., 2017a, MNRAS, 473, 4077
Pillepich A. et al., 2017b, MNRAS, 475, 648
Quai S., Hani M. H., Ellison S. L., Patton D. R., Woo J., 2021, MNRAS, 504, 1888
Rey M. P., Pontzen A., Saintonge A., 2019, MNRAS, 485, 1906
Rodriguez-Gomez V. et al., 2015, MNRAS, 449, 49
Rodriguez-Gomez V. et al., 2016, MNRAS, 458, 2371
Rodriguez-Gomez V. et al., 2017, MNRAS, 467, 3083
Rousseeuw P. J., 1987, J. Comput. Appl. Math., 20, 53
Schawinski K. et al., 2014, MNRAS, 440, 889
Schaye J. et al., 2014, MNRAS, 446, 521
Shlens J., 2014, preprint (arXiv:1404.1100)
Sparre M. et al., 2015, MNRAS, 447, 3548
Springel V. et al., 2017, MNRAS, 475, 676
The IllustrisTNG Project, 2019, IllustrisTNG Public Data Access
Tojeiro R. et al., 2012, MNRAS, 424, 136
Tojeiro R. et al., 2017, MNRAS, 470, 3720
Trayford J. W., Theuns T., Bower R. G., Crain R. A., del P. Lagos C., Schaller M., Schaye J., 2016, MNRAS, 460, 3925
Villforth C. et al., 2014, MNRAS, 439, 3342
Wake D. A. et al., 2006, MNRAS, 372, 537
Wang K., Mao Y.-Y., Zentner A. R., Lange J. U., van den Bosch F. C., Wechsler R. H., 2020, MNRAS, 498, 4450
Wechsler R. H., Tinker J. L., 2018, ARA&A, 56, 435
Weigel A. K. et al., 2017, ApJ, 845, 145
Wild V. et al., 2014, MNRAS, 440, 1880
Wild V. et al., 2020, MNRAS, 494, 529
Wilkinson C. L., Pimbblet K. A., Stott J. P., 2017, MNRAS, 472, 1447
Yoon Y., Im M., Kim J.-W., 2017, ApJ, 834, 73
Zehavi I. et al., 2005, ApJ, 630, 1
Zhu G., 2016, preprint (arXiv:1612.06037)
Zinger E. et al., 2020, MNRAS, 499, 768

This paper has been typeset from a TEX/LATEX file prepared by the author.